Direct Production of a Hyperpolarised Metabolite on a Microfluidic Chip

Sylwia J Barker,[†] Laurynas Dagys,[†] William Hale,[†,¶] Barbara Ripka,[†] James Eills,[‡,§] Manvendra Sharma,[†] Malcolm H Levitt,[†] and Marcel Utz[*,†]

[†]*School of Chemistry, University of Southampton, Southampton, United Kingdom*

[‡]*Institute for Physics, Johannes Gutenberg University, D-55090 Mainz, Germany*

[¶]*Department of Chemistry, University of Florida, Gainesville, USA*

[§]*GSI Helmholtzzentrum für Schwerionenforschung GmbH, Helmholtz-Institut Mainz, 55128 Mainz, Germany*

E-mail: marcel.utz@soton.ac.uk

Abstract

Microfluidic systems hold great potential for the study of live microscopic cultures of cells, tissue samples, and small organisms. Integration of hyperpolarisation would enable quantitative studies of metabolism in such volume limited systems by high-resolution NMR spectroscopy. We demonstrate, for the first time, the integrated generation and detection of a hyperpolarised metabolite on a microfluidic chip. The metabolite [1-^{13}C]fumarate is produced in a nuclear hyperpolarised form by (i) introducing para-enriched hydrogen into the solution by diffusion through a polymer membrane, (ii) reaction with a substrate in the presence of a ruthenium-based catalyst, and (iii) conversion of the singlet-polarised reaction product into a magnetised form by the application of a radiofrequency pulse sequence, all on the same microfluidic chip. The microfluidic device delivers a continuous flow of hyperpolarised material at the 2.5 μL/min scale, with a polarisation level of 4%. We demonstrate two methods

for mitigating singlet-triplet mixing effects which otherwise reduce the achieved polarisation level.

Introduction

Nuclear magnetic resonance (NMR) is a versatile spectroscopic technique, well-suited for noninvasively probing complex chemical systems and their dynamic behaviour. The sensitivity of NMR is limited by the polarisation of nuclear spins, which is small in thermal equilibrium even at the largest available magnetic fields. Hyperpolarisation methods such as parahydrogen-induced polarisation (PHIP)[1–5] can produce much larger spin alignments in special cases, offering several orders of magnitude enhancements in sensitivity. This is particularly attractive in the context of microfluidic lab-on-a-chip (LoC) devices, where sample volumes are typically of the order of nL to µL.[6] Such LoC are versatile platforms on which chemical and biological systems can be studied under precisely controlled and reproducible conditions. LoC systems are commonly used as scaffolds for cell[7–11] and organ[12–15] culture, providing valuable models for supporting the development of diagnostics,[16,17] therapies[12] and drug safety testing,[18,19] but also for chemical reaction monitoring.[20] While state-of-the-art micro-NMR probes can provide ^{1}H NMR detection sensitivities of around 1 nmol$\sqrt{\text{s}}$ for microliter-scale samples in a 14 T magnet at thermal equilibrium,[21] this can be improved into the range of pmol$\sqrt{\text{s}}$ by PHIP.[22] Like other hyperpolarisation methods, PHIP requires specific chemical processes and spin manipulations to produce hyperpolarised species. LoC devices can be used to implement some or all of these processes, thus offering the possibility to integrate production and application of hyperpolarised species in a single, compact platform.

PHIP is conventionally implemented by bubbling hydrogen gas enriched in the para spin isomer through a solution containing a suitable substrate and catalyst, either directly at high magnetic field (PASADENA experiments)[23] or outside of the magnet at low (μT) fields, followed by an adiabatic increase of the magnetic field (ALTADENA experiments).[24] Such experiments are effective, but quite difficult to repeat accurately. This complicates systematic studies of the interplay between

reaction kinetics and nuclear spin relaxation processes. As we have recently shown, microfluidic implementation of PHIP at high field allows delivery of the hydrogen gas by diffusion through a membrane, such that no bubbling is required.[22] Experiments can therefore be carried out under continuous flow, with a stable stationary level of hyperpolarisation established in the chip. This can be exploited for hyperpolarised multidimensional NMR experiments, which require superposition of many transients that must maintain a high level of consistency.

In the following, we use the same approach to probe the formation of hyperpolarised [1-^{13}C]fumarate from [1-^{13}C]disodium acetylenedicarboxylate in an aqueous solution. To our knowledge, this is the first demonstration of PHIP-hyperpolarised metabolite production in a microfluidic device. Hyperpolarised fumarate is widely used as a contrast agent for in-vivo detection of necrosis.[25–34] While the current implementation is not yet ready for use with biological systems due to the presence of the catalyst and other residues, the stability of the microfluidic implementation allows systematic studies of complex kinetic effects.

In this work we generate and observe solutions of [1-^{13}C]fumarate formed via trans-hydrogenative PHIP in a microfluidic chip under continuous-flow conditions, performing the chemical reaction in one part of the chip and NMR detection in another. The operation of this device has been discussed in detail elsewhere.[35] Briefly, all of our experiments are performed inside of a high field NMR spectrometer where the reaction solution containing the precursor and catalyst is delivered to the chip via a syringe pump. Parahydrogen is delivered through a separate channel and diffuses through the PDMS membrane to dissolve into the precursor solution; hence the hydrogenation reaction takes place in the chip.

Microfluidic technology provides a convenient platform for studying hyperpolarised NMR experiments for the following reasons:[6]

1. The results are more reproducible since hydrogen is brought into solution via diffusion through a membrane, which is less erratic than bubbling or shaking.[22,36–38]

2. The reaction kinetics and relaxation properties do not vary between or during experiments since a steady-state can be established between the rate of reaction and relaxation, and this

can be finely tuned by, e.g., varying the flow rates used.[22,36–38]

3. The low volumes used in microfluidics (in this work a few microlitres) makes it more practical to work with expensive or rare samples.

4. Since fresh reaction solution is continually provided to the detection chamber, the samples do not need to be replaced between experiments.[22,37]

5. Bringing the hyperpolarisation step close to the point of detection minimises the signal losses due to relaxation.

Singlet-triplet mixing has been reported to hinder the achievable polarisation of [1-^{13}C]fumarate at high field.[33,39,40] Using our PHIP-on-a-chip system, we quantify how effectively two different RF pulse methods mitigate the problem of ST mixing and support our finding with computational spin dynamics simulations. We present quantitative data on the kinetics and yield of [1-^{13}C]fumarate from [1-^{13}C]disodium acetylenedicarboxylate in a microfluidic device.

Background

The reaction shown in Fig. 1a produces [1-^{13}C]fumarate **II** by hydrogenation of [1-^{13}C]disodium acetylenedicarboxylate **I** with parahydrogen in the presence of a ruthenium catalyst. The slight magnetic inequivalence due to the difference in ^{1}H-^{13}C J-couplings makes it possible to convert the singlet order into observable hyperpolarised magnetisation through the use of RF pulse sequences. In this work we use the singlet-to-magnetisation (S2M) pulse sequence for this task (see Fig. 1e), which is robust against field inhomogeneities in contrast to alternative methods.[41] This is important because magnetic field inhomogeneities are present in the chip due to differences in magnetic susceptibility of the chip and the solvent.[42] Applying this sequence after the chemical reaction with parahydrogen results in high magnetisation of the two protons giving rise to a hyperpolarised substance **II***.

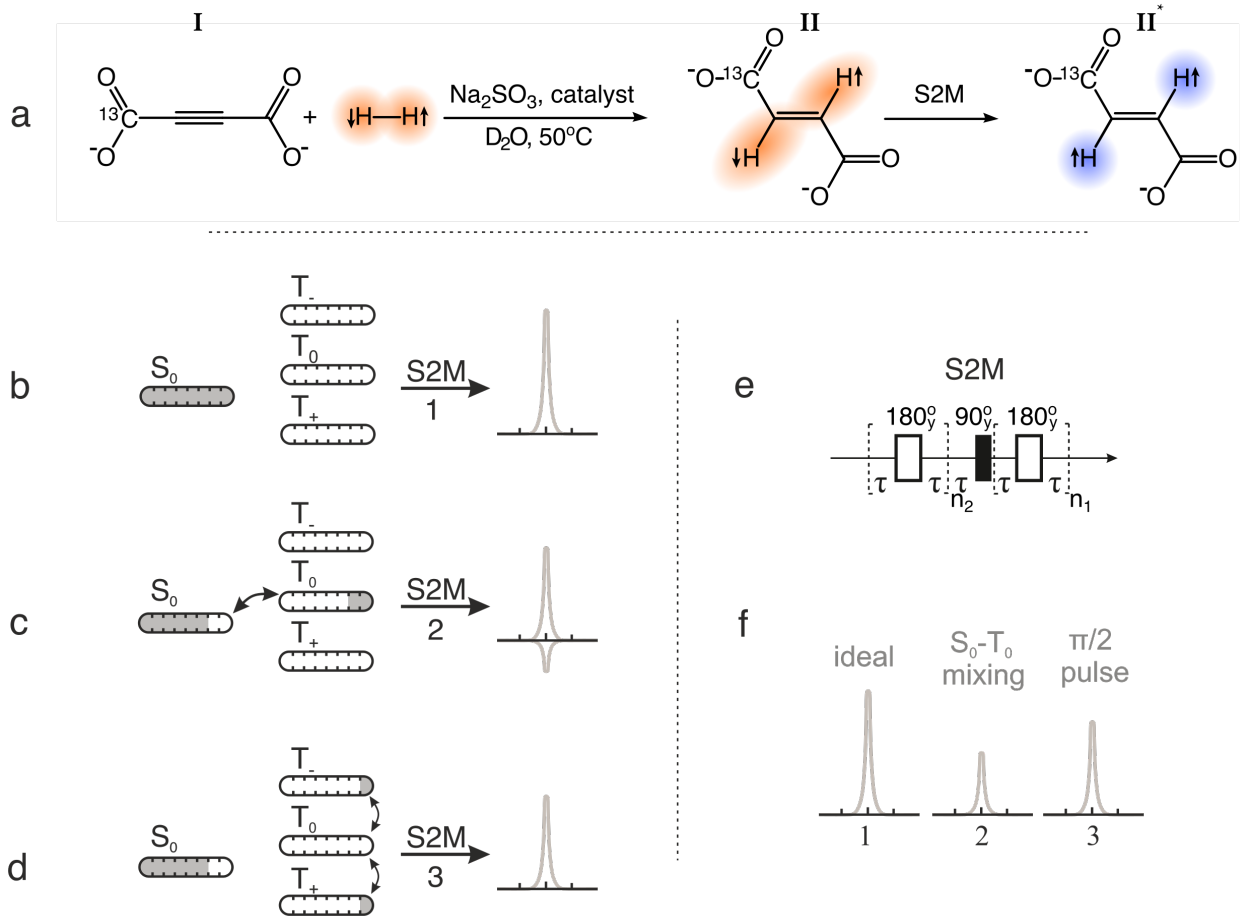

Figure 1: a) Scheme of the reaction investigated in this work. [1-^{13}C]disodium acetylenedicarboxylate labelled as molecule **I** reacts with parahydrogen in the presence of sodium sulfite and the catalyst $[RuCp^*(CH_3CN)_3]PF_6$ in D_2O at 50°C. The reaction results in a production of [1-^{13}C]disodium fumarate, molecule **II**, with the two protons in a singlet state. Application of the S2M pulse sequence converts the singlet state into a state that is magentic and hence observable, molecule **II***. b) Illustration of an ideal case where no ST mixing occurs; only $|S_0\rangle$ state is populated. c) A case where ST mixing occurs leading to a leak of $|S_0\rangle$ state population to the $|T_0\rangle$ state. d) A case where the ST mixing is negated by applying a purge pulse prior the S2M, which distributes the population of $|T_0\rangle$ state to $|T_+\rangle$ and $|T_-\rangle$ states. e) S2M pulse sequence converts the singlet order into observable hyperpolarised magnetisation. The optimal parameters for this molecular system are: $\tau = 15.6$ ms, $n_2 = 14$, $n_1 = 7$. f) Predicted signal intensities for three different scenarios.

The polarisation that is generated on the target molecules can be attenuated by singlet-triplet (ST) mixing (sometimes called ST leakage).[43] The hydrogen molecules can form intermediate hydride species with the catalyst metal center, where the two hydrogen atoms take up inequivalent positions, such that they experience a chemical shift difference at high field. If the lifetime of

this intermediate complex is long enough, there can be a significant leakage from the H_2 proton singlet state ($|S_0\rangle$) to the central triplet state ($|T_0\rangle$), which generally reduces the resulting PHIP signals.[43–45] The S2M sequence converts both the $|S_0\rangle$ and the $|T_0\rangle$ states to magnetisation, but with opposite phases. The population of the $|T_0\rangle$ state therefore *reduces* the resulting NMR signal, as illustrated in Fig. 1b and c. This process sometimes gives rise to a partially-negative line (PNL) in the ^{1}H NMR spectra.[46] It is also known to occur in non-hydrogenative PHIP experiments, and has been noted to give rise to 'spontaneous' polarisation on the target molecules,[47] although generally ST mixing is undesirable.

Two methods have been shown to suppress ST mixing: spin locking on the ^{1}H hydride resonance during the chemical reaction,[39,46,48–56] and applying a hard $\pi/2$ purge pulse to deplete the $|T_0\rangle$ state prior to the polarisation transfer step.[46,52,55–59] These two methods are illustrated in Fig. 1d.

As we show in the following, the study of ST mixing is greatly facilitated by microfluidic PHIP, since instabilities associated with bubbling experiments are avoided. Additionally, since hydrogenative PHIP relies on irreversible chemical reactions, the chemical kinetics influence the observed spectra, and the sample under study would need to be replaced upon the reaction reaching completion. This is a particular issue if the samples are scarce or expensive due to isotopic enrichment. Finally, since hyperpolarised nuclei are in a non-equilibrium state, the NMR signals relax on a timescale of seconds to tens of seconds, unique to each molecular species and nuclear spin site, which can convolute the observed results. This is especially problematic if the signals relax quickly compared to the time it takes for a shaken tube to be placed in the NMR magnet, or for bubbles to settle in solution.

Materials and Methods

All experiments were performed in a 11.7 T magnet using a Bruker AVANCE III spectrometer system. The NMR experiments were performed with a custom-built probe delivering ^{1}H RF pulses

of 125 kHz amplitude.[21] ^{1}H spectra were collected with a 16 ppm spectral width and 8 k point density.

Para-enriched hydrogen gas (gas purity 99.995%) was continuously produced by a Bruker parahydrogen generator BPHG90, with a specified parahydrogen content of 89%.

All chemical compounds were purchased from Sigma Aldrich (United Kingdom) and were used as received. All NMR experiments were performed using a precursor solution of 100 mM [1-^{13}C]disodium acetylenedicarboxylate, 6 mM $[RuCp^{*}(CH_3CN)_3]PF_6$ catalyst and 200 mM sodium sulfite dissolved in D_2O at 50°C. It's been reported that sodium sulfite improves the selectivity of the trans hydrogenation reaction, although the mechanism of its action is not yet known.[33,60]

Microfluidic device

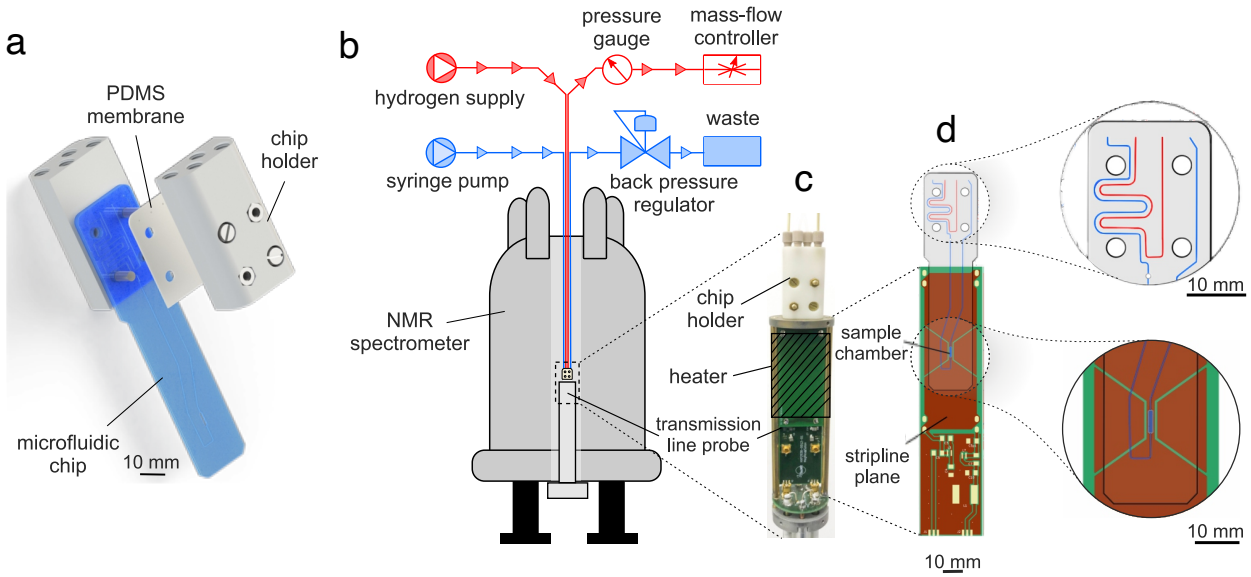

Figure 2: a) Microfluidic chip assembly. b) A schematic diagram of the experimental setup. c) Transmission line probe with the heater indicated as the shaded area. d) Drawing of the microfluidic device aligned with the stripline plane of the detector. The key areas of the drawing are enlarged.

The microfluidic device was made from three layers of polycarbonate (PC) (Self Adhesive Supplies, United Kingdom) with 0.25, 0.5, and 0.25 mm thickness for the top, middle, and bottom layers, respectively. The layers were cut from PC sheets by a LS3040 CO_2 laser cutter (HPC

Laser Ltd, United Kingdom), and were thermally bonded together as described elsewhere.[61] A semi-permeable polydimethylsiloxane (PDMS) membrane of 1 mm thickness (Shielding Solutions, United Kingdom) was placed over the top half of the chip to seal the channels, but allow hydrogen diffusion from the gas channel to the liquid channel. The chip and membrane were held together by 3D printed holders (ProtoLabs, United Kingdom) that attach threaded connectors for 1/16“ capillaries (Cole-Parmer, United Kingdom) to the four access points on the chip for gas and liquid inlets and outlets.

In the magnet, the device was placed in a home-built transmission line probe as shown in Fig. 2c. A heater was clamped outside of the stripline planes to heat the sample chamber in the microfluidic chip to 50°C. This is indicated by the shaded area in Fig. 2c. The heated area did not include the 3D printed holders so that the solution in contact with the hydrogen gas was kept at lower temperature in order to maximise the solubility of the hydrogen gas. The reaction products were detected in a 2.5 μL sample chamber. The chamber of the chip was aligned with the constrictions of the stripline detector as shown in Fig. 2d .[21]

Experimental Procedure

All experiments were performed inside the high-field NMR spectrometer as shown in Fig. 2b. Experiments were conducted at 50°C (at the sample chamber only) with the supply of hydrogen gas set to a pressure of 5 bar and flow rate of 10 mL min^{-1}, stabilised by a mass flow controller (Cole-Parmer, United Kingdom) connected at the end of the line. The flow of the precursor solution was controlled with a syringe pump (Cole-Parmer, United Kingdom) located outside the spectrometer. The target flow rate was set to 10 μL min^{-1}. Under these operating conditions, the NMR signal reached a steady-state after 10 minutes.

Proton singlet order in [1-^{13}C]fumarate was converted into observable magnetisation using the singlet-to-magnetisation (S2M) pulse sequence shown in Fig. 1e. Maximum efficiency was achieved using the following parameters: $\tau = 15.6$ ms, $n_2 = 14$, $n_1 = 7$. The repetition delay was set to 60 s.

CW-S2M experiments were performed by applying continuous wave irradiation for 20 s at 0.5 and 2 kHz, while changing the resonance offset from 20 to -20 ppm. θ-S2M experiments were performed by applying a hard pulse of varying flip angle prior the S2M pulse sequence. This was achieved by varying the pulse duration from 0 to 8 μs in steps of 0.22 μs.

Reference spectrum was obtained using hydrogen in thermal equilibrium. The ^{1}H spectrum was obtained by applying a $\frac{\pi}{2}$ pulse and averaging over 400 scans with a recycle delay of 20 s.

Results and Discussion

Fig. 3a depicts a single-scan proton NMR spectrum obtained after application of the S2M pulse sequence in a steady-state flow experiment with 89% para-enriched H_2. This can be compared to the 400-scan reference spectrum obtained after application of a $\pi/2$ pulse using hydrogen in thermal equilibrium (i.e., not *para*-enriched) in Fig. 3b.

The spectra contain a peak at 6.6 ppm that corresponds to the fumarate protons H^a. From the ratio of the signal intensity in the reference and hyperpolarised spectra, the ^{1}H polarisation was estimated. Accounting for the difference in the number of scans, the signal enhancement was calculated as 190 ± 10. At the field of 11.7 T and temperature of 50°C this corresponds to $0.7 \pm 0.1\%$ ^{1}H polarisation. At 10 μL min^{-1} flow rate, the concentration of fumarate was 1.2 $\pm$ 0.5 mM , which corresponds to 1.2 ± 0.5 % yield. This was calculated by comparing the intensity of the Cp^* peak in the reference spectrum to the intensity of the fumarate peak and accounting for the difference in the number of protons.

The hyperpolarised spectrum features the aforementioned partially negative line at 4 ppm labelled $o - H_2$. The heavy metal catalyst and dissolved molecular hydrogen form intermediate complexes where the two hydrogen nuclei occupy chemically inequivalent positions. At high magnetic field this introduces a chemical shift difference between the two protons, which causes singlet state population to leak into the population of the central triplet state. In addition, the chemical shift difference lifts the degeneracy of the two triplet state transitions. In rapid exchange, this leads to a

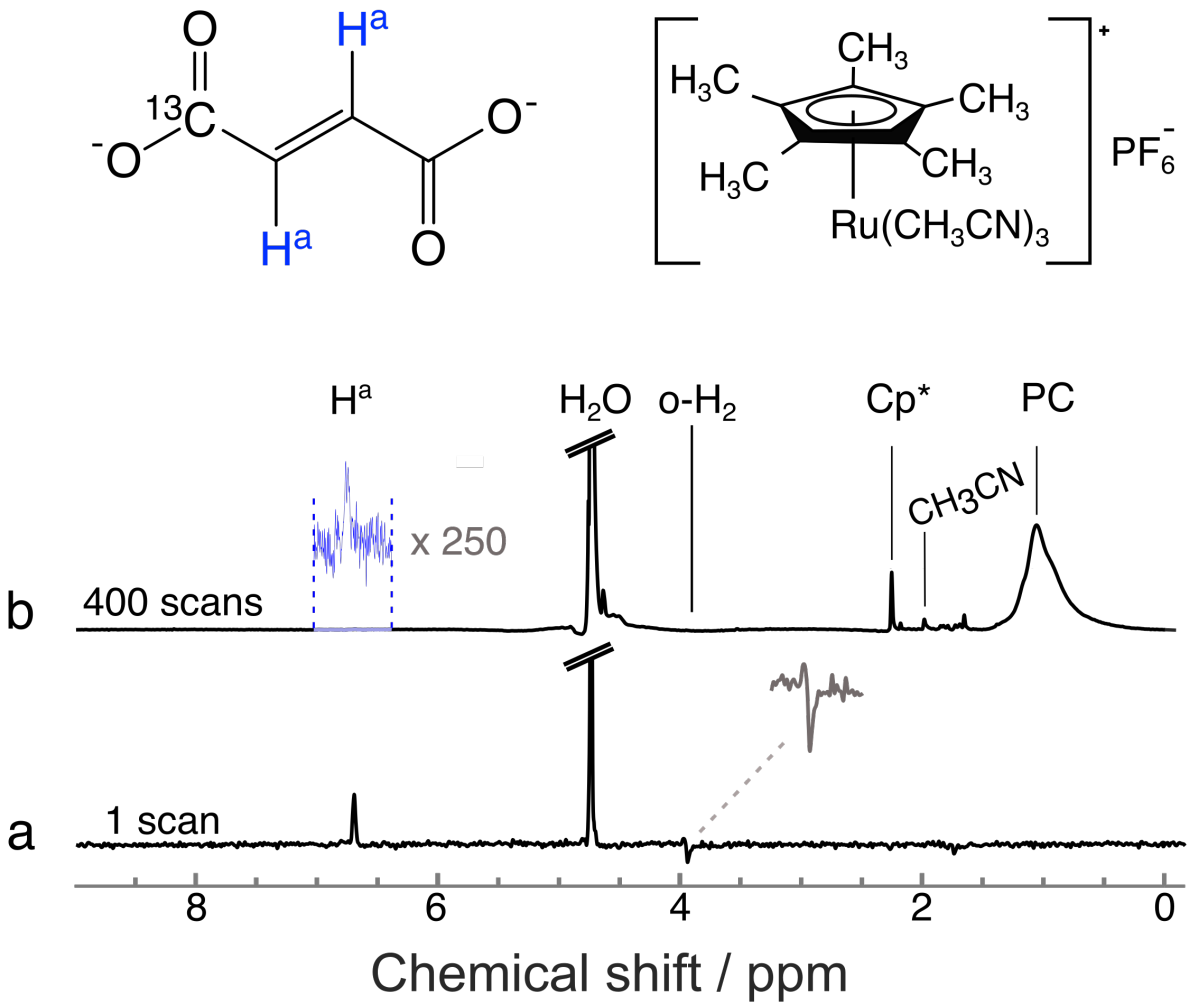

Figure 3: Steady state ^{1}H NMR spectra of [1-^{13}C]fumarate sample flowing at 10 μL min^{-1} in a microfluidic device. a) Spectrum collected with the S2M pulse sequence with 89% parahydrogen. The trace displays a hyperpolarised [1-^{13}C]fumarate peak at 6.6 ppm. The presence of exchanging hydrogen species is indicated at 4 ppm (o $-$ H_2). b) Reference spectrum resulting from a $\pi/2$ pulse with hydrogen in thermal equilibrium. Cp*: catalyst methyl protons, PC: background signal from the polycarbonate chip material.

small partially negative line in the dissolved H_2 signal,[46,47,54,57] as displayed in the spectrum in Fig. 3a.

To suppress the effects of ST mixing we performed experiments in which we applied continuous-wave (CW) irradiation to the sample for 20 s prior to the application of S2M and signal acquisition. The pulse sequence is shown in Fig. 4a. The resulting integral of fumarate signal intensity at 6.6 ppm is plotted as a function of CW offset frequency in Fig. 4b. Experiments were performed

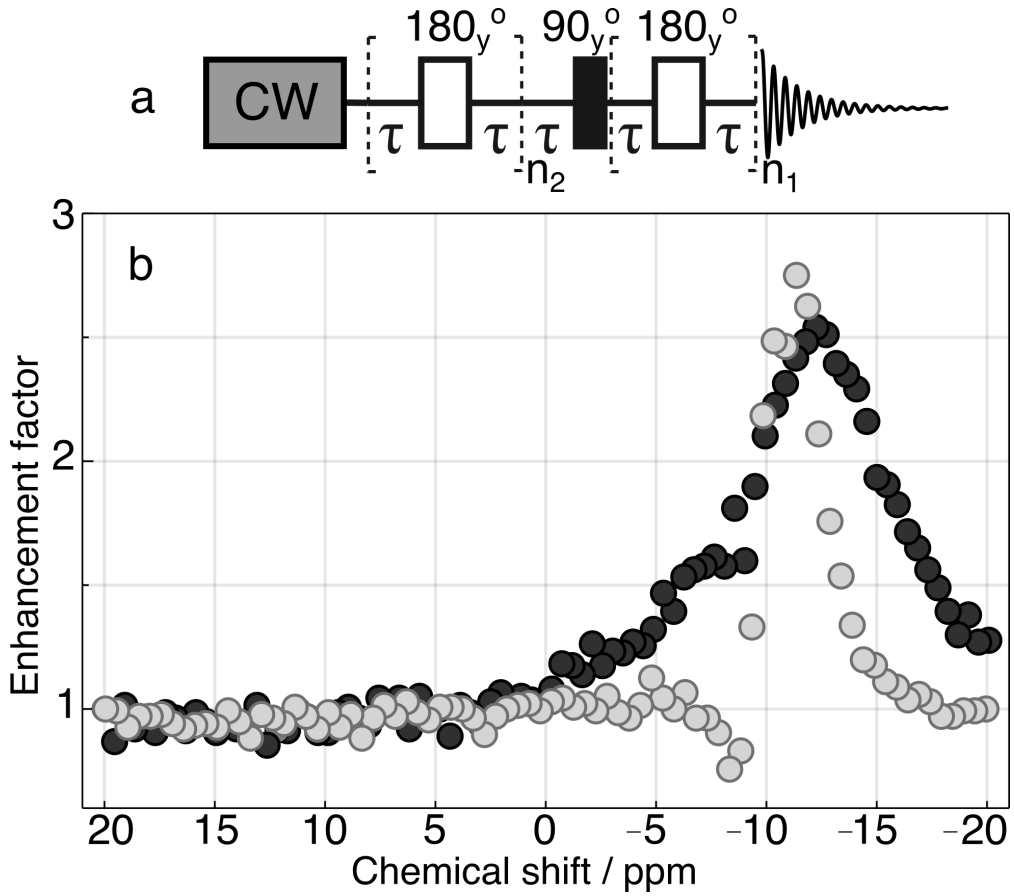

Figure 4: a) Singlet-to-magnetisation pulse sequence with spin-locking field applied during recycle delay. b) Integral of signal intensity of the hyperpolarised proton of [1-^{13}C]disodium fumarate as a function of the resonance offset of the spin-locking field. Experiments were preformed with two CW amplitudes, corresponding to 2 kHz and 0.5 kHz nutation frequency shown as black and grey data points, respectively. Signal amplitude was normalised to the signal acquired with CW frequency set to 20 ppm.

with two different CW amplitudes, corresponding to 0.5 kHz and 2 kHz nutation frequency on protons shown as grey and black circles, respectively.

The profiles of signal intensity against the CW irradiation frequency display a peak at around -11 ppm. This is a typical chemical shift of hydride species for ruthenium complexes,[62] indicating that ST mixing does indeed occur for the hydride species, and is suppressed by CW irradiation. The ^{1}H spectra can be used to observe ST mixing and this has been shown in case of SABRE by either applying a single hard pulse after CW irradiation or a pulse sequence designed to probe higher spin-order if hydride species undergo very fast chemical exchange.[46,47] In the present case,

hydride species are not directly observable due to fast exchange and low sensitivity. The signal is enhanced by a factor of ∼3 when the spin-locking amplitude is set to either to 0.5 kHz or 2 kHz applied at −11 ppm. The peak width in each case corresponds roughly to the excitation bandwidth, resulting in a narrower peak at the lower CW amplitude.

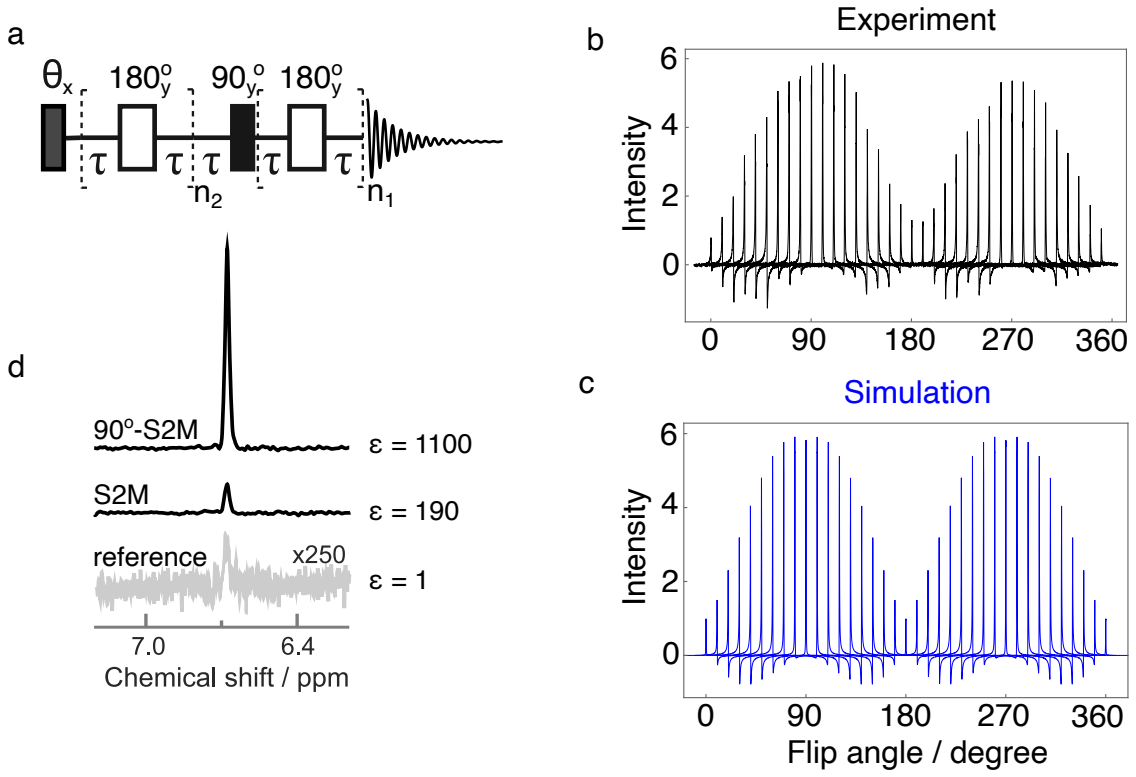

Figure 5: a) θ - S2M pulse sequence. The θ angle was arrayed from 0° to 360° in steps of 10°. $\tau = 15.6$ ms, $n_1 = 7$, $n_2 = 14$. b) Experimentally obtained H^a signals of [1-^{13}C]fumarate as a function of the purge pulse angle. The y-axis shows the improvement of the enhancement factor compared to S2M without the purge pulse. c) Computational simulation of the spin system using SpinDynamica software.[63] d) Comparison of the signal intensity of fumarate protons (H^a) between the reference spectrum, pure S2M and 90° − S2M.

We contrast this to another method, which has been used to address ST mixing effects: applying a hard pulse (which we will refer to as the purge pulse) to the protons prior to polarisation transfer and signal acquisition. Application of a $\pi/2$ purge pulse on the proton channel depletes the $|T_0\rangle$ state, which partially reconstitutes the population difference between the $|S_0\rangle$ and $|T_0\rangle$ states [46,52,55,57–59].

Fig. 5a shows the pulse sequence used to investigate the phenomenon, and Fig. 5b shows the hyperpolarised H^a proton signals obtained experimentally by varying the flip angle θ. The flip angle was varied from 0° to 360° in steps of 10°. The signal shows an oscillatory dependence on the flip angle of the purge pulse, with maxima occurring at 90° and 270°, and no improvement seen near 180°. The signal at 270° is about 15% less than at 90°. While this is likely due to B_1 inhomogeneities, other factors, for example chemical kinetics on the timescale of the pulse length, may also contribute.

The spectral peaks in Fig. 5 also display phase distortions depending on the flip angle of the purge pulse. The origin of the effect was confirmed by numerical simulations using software package SpinDynamica[63] and the result is shown in Fig. 5c. The simulation assumes that before the application of the sequence depicted in Fig. 5a, the $|\mathrm{S}_0\rangle$ and $|\mathrm{T}_0\rangle$ states are 55% and 45% populated, respectively. The populations of the other triplet states are neglected. The agreement between experimental data and numerical simulation is striking. Both experiments and simulations show phase distortions when the flip angle is not an integer multiple of 90 degrees. These phase distortions arise as follows: When the first pulse has a flip angle of 90 degrees, the pulse transfers the population of the central triplet state $|T_0\rangle$ to the outer triplet states $|T_{\pm1}\rangle$, increasing the population difference between the singlet state $|S_0\rangle$ and the central triplet state $|T_0\rangle$, and hence enhancing the hyperpolarised NMR signal at the end of the pulse sequence. However, the flip angle of the first pulse is not a multiple of 90 degrees, the transport of populations between the triplet state is accompanied by the excitation of single-quantum triplet-triplet coherences, of the form $|T_{\pm1}\rangle\langle T_0|$ and $|T_0\rangle\langle T_{\pm1}|$. These coherences persist throughout the pulse sequence, and appear as out-of-phase signal components in the observed spectrum, which have the effect of an undesirable phase shift of the observed peak.

In Fig. 5d a comparison is shown between the reference spectrum obtained with 400 scans and single scan NMR spectra of protons H^a after applying the S2M sequence with a purge pulse of 0° and 90°. The enhancement in the latter case was calculated to be 1100 ± 10 in contrast to 190 ± 10 without applying the purge pulse. This corresponds to $4.0 \pm 0.1\%$ ^{1}H polarisation, and hence a

nearly 6-fold improvement in achievable fumarate signal. The enhancement factor was calculated by comparing the integral of the H^a peak in the hyperpolarised and reference spectrum, accounting for the difference in the number of scans between the two spectra.

The hard-pulse method yielded a 6-fold improvement in the achievable fumarate signal, compared to 3 for the spin-locking method. This was unexpected since the spin-locking method can in principle lead to higher signal enhancements as it should mitigate the effect of ST mixing entirely. We believe the lower efficiency provided by spin locking is due to the micro-NMR probe design where the RF field is concentrated exclusively onto the sample chamber as shown in Fig. 2d. Therefore the solution outside the sample chamber is not affected by the RF irradiation, and thus the ST mixing cannot be suppressed for molecules of fumarate that formed in the channels before reaching the sample chamber. This is not a problem for the hard-pulse method since the pulse is applied after the chemical reaction.

The results obtained show the remarkable reproducibility and stability of the chemical reactions performed in the microfluidic device over the course of hours. A steady-state between the rate of chemical reaction to form the hyperpolarised product and the rate of relaxation was established, and without the confounding influence of these external factors it is possible to study and optimise pulse sequences in hyperpolarised NMR experiments. An additional benefit of working on a microfluidic scale is the small sample volumes required, meaning expensive or scarce samples can be more readily used. For example, the data in Fig. 5b required 40 minutes of experimental time, consuming 400 μL of solution, which is the approximate volume required for a single PHIP experiment in a conventional 5 mm NMR tube.

The yield of fumarate in the chip was 1.2 ± 0.5 %. The low yield of the reaction is most likely due to the limited uptake of hydrogen into the flowing solution. Finite element simulations of the chip have shown that when methanol is flowed through the chip at $10\,\mu\mathrm{L\,min^{-1}}$ at pressure of 5 bar, only 10 mM of hydrogen dissolves in the fluid.[64] Since in this work water was used as the solvent, the concentration of hydrogen dissolved is expected to be lower due to poorer solubility of hydrogen in water. Modifications to the apparatus to improve the H_2 uptake and yield of the

reaction are currently underway.

Conclusion

In this work we employed a microfluidic chip to run PHIP reactions, incorporating the hydrogenation, sample transport, RF excitation and signal detection steps onto a single device. In the reaction we hyperpolarised [1-^{13}C]fumarate, and used the S2M pulse sequence to generate in-phase proton magnetisation for observation in the 2.5 μL sample chamber, achieving 4% proton polarisation. We used this system to investigate pulsed NMR methods that reduce the detrimental effects of singlet-triplet mixing in this PHIP reaction. We showed that application of continuous wave irradiation prior to applying the S2M pulse sequence leads to a 3-fold improvement to the fumarate proton polarisation, and also allowed us to locate the chemical shift of the catalyst complex on which singlet-triplet mixing occurs. We contrasted that with application of a $\pi/2$ pulse prior to applying the S2M sequence, which led to a 6-fold improvement to the proton polarisation.

This continuous-flow PHIP approach allows one to establish a constant stream of a hyperpolarised product, providing stable and reproducible conditions for the study of complex chemical and spin-dynamical phenomena in a well-controlled environment. This is an important step towards observation of metabolism in biological systems by hyperpolarised NMR on a single microfluidic device. By bringing hydrogen gas into solution through a membrane as opposed to bubbling or shaking, the chemical reaction is more stable and reaches a steady-state with a variation in the concentration of reaction product of 1%. By operating at a small volume-scale (microliters), the consumption of expensive materials is significantly reduced as compared to performing reactions in NMR tubes.

Not only does microfluidic implementation aid in the development of hyperpolarised NMR methods, but incorporating hyperpolarisation to enhance NMR signals opens the door to the use of NMR as a detection method to study biological systems in microfluidic devices. Methods such as fluorescence spectroscopy require using specific fluorescent tags to track molecules, and UV-

visible spectroscopy offers limited ability to identify molecules. The molecular specificity and non-destructive nature of NMR spectroscopy makes it an ideal technique to track metabolic reactions, and direct production of hyperpolarised fumarate in a microfluidic chip is an important step towards this goal. However, further developments are required to make this dream a reality, such as the removal of toxic chemicals after the hyperpolarisation process, and the incorporation of ^{13}C NMR for background-free detection with high chemical specificity and resolution.

Much work with hyperpolarised biomolecules relies on ^{13}C hyperpolarisation and detection, since this is preferable for *in vivo* imaging as the large background signals from water molecules are not present. The probe used for this work is doubly tuned for ^{1}H and ^{13}C excitation and detection but in order to perform such experiments several issues need to be addressed. A prerequisite of using PHIP-polarised metabolites for biological studies is the ability to remove the catalyst and reaction side-products from the solution. This has been shown to be possible for [1-^{13}C]fumarate via a precipitation procedure,[32] and for a variety of other PHIP-polarised metabolites via the side-arm hydrogenation procedure.[55] Precipitation procedures are not feasible in microfluidic devices as the solid would block the fluidic channels. However, scavenger compounds that bind the catalyst could potentially be used for this purpose.[65,66]

Acknowledgement

The authors are indebted to Dr. Christian Bengs and Dr. Giuseppe Pileio for help with the SpinDynamica simulations, as well as for insightful discussions about the results and theory. This work has been supported by an EPSRC iCASE studentship EP/R513325/1 to SJB, co-funded by Bruker UK Ltd., as well as by the EU H2020 FETOpen Project "TISuMR" (Grant number 737043). This project has also received funding from the European Union's Horizon 2020 research and innovation programme under the Marie Skłodowska-Curie Grant Agreement No. 766402, as well as ERC project 786707-FunMagResBeacons, and EPSRC grants EP/P009980/1 and EP/V055593/1.

References

(1) Natterer, J.; Bargon, J. Parahydrogen induced polarization. *Prog. Nucl. Magn. Reson. Spectrosc.* **1997**, *31*, 293–315.

(2) Adams, R. W.; Aguilar, J. A.; Atkinson, K. D.; Cowley, M. J.; Elliott, P. I. P.; Duckett, S. B.; Green, G. G. R.; Khazal, I. G.; López-Serrano, J.; Williamson, D. C. Reversible interactions with para-hydrogen enhance NMR sensitivity by polarization transfer. *Science* **2009**, *323*, 1708–1711.

(3) Deninger, A. J.; Eberle, B.; Ebert, M.; Großmann, T.; Heil, W.; Kauczor, H. U.; Lauer, L.; Markstaller, K.; Otten, E.; Schmiedeskamp, J.; Schreiber, W.; Surkau, R.; Thelen, M.; Weiler, N. Quantification of Regional Intrapulmonary Oxygen Partial Pressure Evolution during Apnea by 3He MRI. *J. Magn. Reson.* **1999**, *141*, 207–216.

(4) Bowers, C. R.; Weitekamp, D. P. Transformation of symmetrization order to nuclear-spin magnetization by chemical reaction and nuclear magnetic resonance. *Phys. Rev. Lett.* **1986**, *57*, 2645–2648.

(5) Maly, T.; Debelouchina, G. T.; Bajaj, V. S.; Hu, K.-N.; Joo, C.-G.; Mak-Jurkauskas, M. L.; Sirigiri, J. R.; van der Wel, P. C. A.; Herzfeld, J.; Temkin, R. J.; Griffin, R. G. Dynamic nuclear polarization at high magnetic fields. *J. Chem. Phys.* **2008**, *128*, 052211.

(6) Eills, J.; Hale, W.; Utz, M. Synergies between Hyperpolarized NMR and Microfluidics: A Review. *Prog. Nucl. Magn. Reson. Spectrosc.* **2021**,

(7) Patra, B.; Sharma, M.; Hale, W.; Utz, M. Time-resolved non-invasive metabolomic monitoring of a single cancer spheroid by microfluidic NMR. *Sci. Rep.* **2021**, *11*, 53.

(8) Coluccio, M. L.; Perozziello, G.; Malara, N.; Parrotta, E.; Zhang, P.; Gentile, F.; Limongi, T.; Raj, P. M.; Cuda, G.; Candeloro, P.; Di Fabrizio, E. Microfluidic platforms for cell cultures and investigations. *Microelectron. Eng.* **2019**, *208*, 14–28.

(9) Mehling, M.; Tay, S. Microfluidic cell culture. *Curr. Opin. Biotechnol.* **2014**, *25*, 95–102.

(10) Du, G.; Fang, Q.; den Toonder, J. M. J. Microfluidics for cell-based high throughput screening platforms—A review. *Anal. Chim. Acta* **2016**, *903*, 36–50.

(11) Xiong, B.; Ren, K.; Shu, Y.; Chen, Y.; Shen, B.; Wu, H. Recent Developments in Microfluidics for Cell Studies. *Adv. Mater.* **2014**, *26*, 5525–5532.

(12) Wu, Q.; Liu, J.; Wang, X.; Feng, L.; Wu, J.; Zhu, X.; Wen, W.; Gong, X. Organ-on-a-chip: recent breakthroughs and future prospects. *Biomed. Eng. Online* **2020**, *19*, 9.

(13) Jang, K.-J.; Suh, K.-Y. A multi-layer microfluidic device for efficient culture and analysis of renal tubular cells. *Lab Chip* **2010**, *10*, 36–42.

(14) Stucki, A. O.; Stucki, J. D.; Hall, S. R. R.; Felder, M.; Mermoud, Y.; Schmid, R. A.; Geiser, T.; Guenat, O. T. A lung-on-a-chip array with an integrated bio-inspired respiration mechanism. *Lab Chip* **2015**, *15*, 1302–1310.

(15) Mandenius, C.-F. Conceptual Design of Micro-Bioreactors and Organ-on-Chips for Studies of Cell Cultures. *Bioeng.* **2018**, *5*, 56.

(16) Kolluri, N.; M. Klapperich, C.; Cabodi, M. Towards lab-on-a-chip diagnostics for malaria elimination. *Lab Chip* **2018**, *18*, 75–94.

(17) Wu, J.; Dong, M.; Rigatto, C.; Liu, Y.; Lin, F. Lab-on-chip technology for chronic disease diagnosis. *NPJ Digit. Med.* **2018**, *1*, 1–11.

(18) Jodat, Y. A.; Kang, M. G.; Kiaee, K.; Kim, G. J.; Martinez, A. F. H.; Rosenkranz, A.; Bae, H.; Shin, S. R. Human-Derived Organ-on-a-Chip for Personalized Drug Development. *Curr. Pharm. Des* **2018**, *24*, 5471–5486.

(19) Cong, Y.; Han, X.; Wang, Y.; Chen, Z.; Lu, Y.; Liu, T.; Wu, Z.; Jin, Y.; Luo, Y.; Zhang, X. Drug Toxicity Evaluation Based on Organ-on-a-chip Technology: A Review. *Micromachines* **2020**, *11*.

(20) Wu, B.; Ecken, S. v. d.; Swyer, I.; Li, C.; Jenne, A.; Vincent, F.; Schmidig, D.; Kuehn, T.; Beck, A.; Busse, F.; Stronks, H.; Soong, R.; Wheeler, A. R.; Simpson, A. Rapid Chemical Reaction Monitoring by Digital Microfluidics-NMR: Proof of Principle Towards an Automated Synthetic Discovery Platform. *Angew. Chem. Int. Ed.* **2019**, *58*, 15372–15376.

(21) Sharma, M.; Utz, M. Modular transmission line probes for microfluidic nuclear magnetic resonance spectroscopy and imaging. *J. Magn. Reson.* **2019**, *303*, 75–81.

(22) Eills, J.; Hale, W.; Sharma, M.; Rossetto, M.; Levitt, M. H.; Utz, M. High-Resolution Nuclear Magnetic Resonance Spectroscopy with Picomole Sensitivity by Hyperpolarization on a Chip. *J. Am. Chem. Soc.* **2019**, *141*, 9955–9963.

(23) Bowers, C. R.; Weitekamp, D. P. Parahydrogen and synthesis allow dramatically enhanced nuclear alignment. *J. Am. Chem. Soc.* **1987**, *109*, 5541–5542.

(24) Pravica, M. G.; Weitekamp, D. P. Net NMR alignment by adiabatic transport of parahydrogen addition products to high magnetic field. *Chem. Phys. Lett.* **1988**, *145*, 255–258.

(25) Gallagher, F. A.; Kettunen, M. I.; Hu, D.-E.; Jensen, P. R.; In 't Zandt, R.; Karlsson, M.; Gisselsson, A.; Nelson, S. K.; Witney, T. H.; Bohndiek, S. E.; Hansson, G.; Peitersen, T.; Lerche, M. H.; Brindle, K. M. Production of hyperpolarized [1,4-13C2]malate from [1,4-13C2]fumarate is a marker of cell necrosis and treatment response in tumors. *Proc. Natl. Acad. Sci. U.S.A.* **2009**, *106*, 19801.

(26) Witney, T. H.; Kettunen, M. I.; Hu, D.-e.; Gallagher, F. A.; Bohndiek, S. E.; Napolitano, R.; Brindle, K. M. Detecting treatment response in a model of human breast adenocarcinoma using hyperpolarised [1-13C]pyruvate and [1,4-13C2]fumarate. *Br. J. Cancer* **2010**, *103*, 1400.

(27) Bohndiek, S. E.; Kettunen, M. I.; Hu, D.-e.; Witney, T. H.; Kennedy, B. W. C.; Gallagher, F. A.; Brindle, K. M. Detection of Tumor Response to a Vascular Disrupting Agent by Hyperpolarized 13C Magnetic Resonance Spectroscopy. *Mol. Cancer Ther.* **2010**, *9*, 3278–3288.

(28) Clatworthy, M. R.; Kettunen, M. I.; Hu, D.-E.; Mathews, R. J.; Witney, T. H.; Kennedy, B. W. C.; Bohndiek, S. E.; Gallagher, F. A.; Jarvis, L. B.; Smith, K. G. C.; Brindle, K. M. Magnetic resonance imaging with hyperpolarized [1,4-13C2]fumarate allows detection of early renal acute tubular necrosis. *Proc. Natl. Acad. Sci. U.S.A.* **2012**, *109*, 13374–13379.

(29) Mignion, L.; Dutta, P.; Martinez, G. V.; Foroutan, P.; Gillies, R. J.; Jordan, B. F. Monitoring chemotherapeutic response by hyperpolarized 13C-fumarate MRS and diffusion MRI. *Cancer Res.* **2014**, *74*, 686–694.

(30) Miller, J. J.; Lau, A. Z.; Nielsen, P. M.; McMullen-Klein, G.; Lewis, A. J.; Jespersen, N. R.; Ball, V.; Gallagher, F. A.; Carr, C. A.; Laustsen, C.; Bøtker, H. E.; Tyler, D. J.; Schroeder, M. A. Hyperpolarized [1,4- 13 C 2]Fumarate Enables Magnetic Resonance-Based Imaging of Myocardial Necrosis. *JACC Cardiovasc. Imaging* **2018**, *11*, 1594–1606.

(31) Laustsen, C.; Nielsen, P. M.; Qi, H.; Løbner, M. H.; Palmfeldt, J.; Bertelsen, L. B. Hyperpolarized [1,4-13C]fumarate imaging detects microvascular complications and hypoxia mediated cell death in diabetic nephropathy. *Sci. Rep.* **2020**, *10*, 1–10.

(32) Knecht, S. et al. Rapid hyperpolarization and purification of the metabolite fumarate in aqueous solution. *Proc. Natl. Acad. Sci. U.S.A.* **2021**, *118*, e2025383118.

(33) Wienands, L.; Theiß, F.; Eills, J.; Rösler, L.; Knecht, S.; Buntkowsky, G. Optimizing the Reaction Conditions for the Formation of Fumarate via Trans-Hydrogenation. *Appl. Magn. Reson.* **2021**, 1–20.

(34) Eills, J.; Cavallari, E.; Kircher, R.; Di Matteo, G.; Carrera, C.; Dagys, L.; Levitt, M. H.; Ivanov, K. L.; Aime, S.; Reineri, F.; Münnemann, K.; Budker, D.; Buntkowsky, G.; Knecht, S. Singlet-Contrast Magnetic Resonance Imaging: Unlocking Hyperpolarization with Metabolism. *Angew. Chem. Int. Ed.* **2021**, *60*, 6791–6798.

(35) Eills, J.; Cavallari, E.; Carrera, C.; Budker, D.; Aime, S.; Reineri, F. Real-Time Nuclear

Magnetic Resonance Detection of Fumarase Activity Using Parahydrogen-Hyperpolarized [1-13C]Fumarate. *J. Am. Chem. Soc.* **2019**, *141*, 20209–20214.

(36) Lehmkuhl, S.; Wiese, M.; Schubert, L.; Held, M.; Küppers, M.; Wessling, M.; Blümich, B. Continuous hyperpolarization with parahydrogen in a membrane reactor. *J. Magn. Reson.* **2018**, *291*, 8–13.

(37) Bordonali, L.; Nordin, N.; Fuhrer, E.; MacKinnon, N.; Korvink, J. G. Parahydrogen based NMR hyperpolarisation goes micro: an alveolus for small molecule chemosensing. *Lab Chip* **2019**, *19*, 503–512.

(38) Roth, M.; Kindervater, P.; Raich, H.-P.; Bargon, J.; Spiess, H. W.; Münnemann, K. Continuous 1H and 13C signal enhancement in NMR spectroscopy and MRI using parahydrogen and hollow-fiber membranes. *Angew. Chem. Int. Ed.* **2010**, *49*, 8358–8362.

(39) Rodin, B. A.; Kozinenko, V. P.; Kiryutin, A. S.; Yurkovskaya, A. V.; Eills, J.; Ivanov, K. L. Constant-adiabaticity pulse schemes for manipulating singlet order in 3-spin systems with weak magnetic non-equivalence. *J. Magn. Reson.* **2021**, *327*, 106978.

(40) Dagys, L.; Ripka, B.; Leutzsch, M.; Moustafa, G. A. I.; Eills, J.; Colell, J. F. P.; Levitt, M. H. Geminal parahydrogen-induced polarization: accumulating long-lived singlet order on methylene proton pairs. *Magn. Reson.* **2020**, *1*, 175–186.

(41) Pileio, G.; Carravetta, M.; Levitt, M. H. Storage of nuclear magnetization as long-lived singlet order in low magnetic field. *Proc. Natl. Acad. Sci. U.S.A* **2010**, *107*, 17135–17139.

(42) Hale, W.; Rossetto, G.; Greenhalgh, R.; Finch, G.; Utz, M. High-resolution nuclear magnetic resonance spectroscopy in microfluidic droplets. *Lab Chip* **2018**, *18*, 3018–3024.

(43) Kating, P.; Wandelt, A.; Selke, R.; Bargon, J. Nuclear singlet/triplet mixing during hydrogenations with parahydrogen: an in situ NMR method to investigate catalytic reac-

tion mechanisms and their kinetics. 2. Homogeneous hydrogenation of 1,4-dihydro-1,4-epoxynaphthalene using different rhodium catalysts. *J. Phys. Chem* **1993**, *97*, 13313–13317.

(44) Bargon, J.; Kandels, J.; Kating, P. Nuclear magnetic resonance studies of homogeneous catalysis using parahydrogen: Analysis of nuclear singlet–triplet mixing as a diagnostic tool to characterize intermediates. *J. Chem. Phys.* **1993**, *98*, 6150–6153.

(45) Dagys, L.; Bengs, C.; Levitt, M. H. Low-frequency excitation of singlet–triplet transitions. Application to nuclear hyperpolarization. *J. Chem. Phys.* **2021**, *155*, 154201.

(46) Kiryutin, A. S.; Sauer, G.; Yurkovskaya, A. V.; Limbach, H.-H.; Ivanov, K. L.; Buntkowsky, G. Parahydrogen Allows Ultrasensitive Indirect NMR Detection of Catalytic Hydrogen Complexes. *J. Phys. Chem. C* **2017**, *121*, 9879–9888.

(47) Knecht, S.; Kiryutin, A. S.; Yurkovskaya, A. V.; Ivanov, K. L. Mechanism of spontaneous polarization transfer in high-field SABRE experiments. *J. Magn. Reson.* **2018**, *287*, 74–81.

(48) Berner, S.; Schmidt, A. B.; Zimmermann, M.; Pravdivtsev, A. N.; Glöggler, S.; Hennig, J.; von Elverfeldt, D.; Hövener, J.-B. SAMBADENA Hyperpolarization of 13 C-Succinate in an MRI: Singlet-Triplet Mixing Causes Polarization Loss. *ChemistryOpen* **2019**, *8*, 728–736.

(49) Pravdivtsev, A. N. Transfer of SABRE-derived hyperpolarization to spin-1/2 heteronuclei. *RSC Advances* **2015**, 9.

(50) Goldman, M.; Jóhannesson, H.; Axelsson, O.; Karlsson, M. Design and implementation of 13C hyper polarization from para-hydrogen, for new MRI contrast agents. *Comptes Rendus Chimie* **2006**, *9*, 357–363.

(51) Vaneeckhaute, E.; De Ridder, S.; Tyburn, J.-M.; Kempf, J. G.; Taulelle, F.; Martens, J. A.; Breynaert, E. Long-Term Generation of Longitudinal Spin Order Controlled by Ammonia Ligation Enables Rapid SABRE Hyperpolarized 2D NMR. *ChemPhysChem* **2021**, *22*, 1170–1177.

(52) Barskiy, D. A.; Knecht, S.; Yurkovskaya, A. V.; Ivanov, K. L. SABRE: Chemical kinetics and spin dynamics of the formation of hyperpolarization. *Prog. Nucl. Magn. Reson. Spectrosc.* **2019**, *114-115*, 33–70.

(53) Knecht, S.; Ivanov, K. L. Quantitative quantum mechanical approach to SABRE hyperpolarization at high magnetic fields. *J. Chem. Phys.* **2019**, *150*, 124106.

(54) Knecht, S.; Hadjiali, S.; Barskiy, D. A.; Pines, A.; Sauer, G.; Kiryutin, A. S.; Ivanov, K. L.; Yurkovskaya, A. V.; Buntkowsky, G. Indirect Detection of Short-Lived Hydride Intermediates of Iridium N-Heterocyclic Carbene Complexes via Chemical Exchange Saturation Transfer Spectroscopy. *J. Phys. Chem. C* **2019**, 6.

(55) Reineri, F.; Cavallari, E.; Carrera, C.; Aime, S. Hydrogenative-PHIP polarized metabolites for biological studies. *Magn. Reson. Mater. Phys. Biol. Med.* **2021**, *34*, 25–47.

(56) Markelov, D. A.; Kozinenko, V. P.; Knecht, S.; Kiryutin, A. S.; Yurkovskaya, A. V.; Ivanov, K. L. Singlet to triplet conversion in molecular hydrogen and its role in parahydrogen induced polarization. *Phys. Chem. Chem. Phys.* **2021**, *23*, 20936–20944.

(57) Knecht, S.; Kiryutin, A. S.; Yurkovskaya, A. V.; Ivanov, K. L. Efficient conversion of anti-phase spin order of protons into 15N magnetisation using SLIC-SABRE. *Mol. Phys.* **2019**, *117*, 2762–2771.

(58) Theis, T.; Truong, M.; Coffey, A. M.; Chekmenev, E. Y.; Warren, W. S. LIGHT-SABRE enables efficient in-magnet catalytic hyperpolarization. *J. Magn. Reson.* **2014**, *248*, 23–26.

(59) Natterer, J.; Schedletzky, O.; Barkemeyer, J.; Bargon, J.; Glaser, S. J. Investigating Catalytic Processes with Parahydrogen: Evolution of Zero-Quantum Coherence in AA'X Spin Systems. *J. Magn. Reson.* **1998**, *133*, 92–97.

(60) Ripka, B.; Eills, J.; Kouřilová, H.; Leutzsch, M.; Levitt, M. H.; Münnemann, K. Hyperpolarized fumarate via parahydrogen. *ChemComm* **2018**, *54*, 12246–12249.

(61) Yilmaz, A.; Utz, M. Characterisation of oxygen permeation into a microfluidic device for cell culture by in situ NMR spectroscopy. *Lab Chip* **2016**, *16*, 2079–2085.

(62) Rosal, I. d.; Maron, L.; Poteau, R.; Jolibois, F. DFT calculations of 1H and 13C NMR chemical shifts in transition metal hydrides. *Dalton Trans.* **2008**, 3959–3970.

(63) Bengs, C.; Levitt, M. H. SpinDynamica: Symbolic and numerical magnetic resonance in a Mathematica environment. *Magn. Reson. Chem.* **2018**, *56*, 374–414.

(64) Ostrowska, S. J.; Rana, A.; Utz, M. Spatially Resolved Kinetic Model of Parahydrogen Induced Polarisation (PHIP) in a Microfluidic Chip. *ChemPhysChem* **2021**, *22*, 2004–2013.

(65) Barskiy, D. A.; Ke, L. A.; Li, X.; Stevenson, V.; Widarman, N.; Zhang, H.; Truxal, A.; Pines, A. Rapid Catalyst Capture Enables Metal-Free para-Hydrogen-Based Hyperpolarized Contrast Agents. *J. Phys. Chem. Lett.* **2018**, *9*, 2721–2724.

(66) Kidd, B.; Gesiorski, J. L.; Gemeinhardt, M. E.; Shchepin, R. V.; Kovtunov, K. V.; Koptyug, I. V.; Chekmenev, E. Y.; Goodson, B. M. Facile Removal of Homogeneous SABRE Catalysts for Purifying Hyperpolarized Metronidazole, a Potential Hypoxia Sensor. *J. Phys. Chem. C* **2018**, *122*, 16848–16852.

Graphical TOC Entry